

RESEARCH ARTICLE | FEBRUARY 06 2025

## Characterization and bacterial inactivation application of multiple pin-to-plate electrode-based DBD plasma driven by nanosecond-pulsed high voltage

Min-Jeong Seong; Kyu-Ri Park; S. J. Kim ; Hea-Min Joh; Hanul Moon ; T. H. Chung  



*Phys. Plasmas* 32, 023504 (2025)

<https://doi.org/10.1063/5.0241367>



### Articles You May Be Interested In

Assessment of microbial species inactivation and purification of sewage by a gas–liquid diaphragm discharge plasma

*J. Appl. Phys.* (September 2023)

Inactivation of microorganisms in model tissues by plasma-activated gas

*Phys. Plasmas* (August 2024)

Roles of individual radicals generated by a submerged dielectric barrier discharge plasma reactor during *Escherichia coli* O157:H7 inactivation

*AIP Advances* (October 2015)

07 February 2025 02:35:46



Physics of Plasmas

Special Topics Open  
for Submissions

[Learn More](#)



# Characterization and bacterial inactivation application of multiple pin-to-plate electrode-based DBD plasma driven by nanosecond-pulsed high voltage

Cite as: Phys. Plasmas **32**, 023504 (2025); doi: 10.1063/5.0241367

Submitted: 30 September 2024 · Accepted: 17 January 2025 ·

Published Online: 6 February 2025



View Online



Export Citation



CrossMark

Min-Jeong Seong, Kyu-Ri Park, S. J. Kim,  Hea-Min Joh, Hanul Moon,  and T. H. Chung<sup>a)</sup> 

## AFFILIATIONS

Department of Physics, Dong-A University, Busan 49315, South Korea

<sup>a)</sup> Author to whom correspondence should be addressed: [thchung@dau.ac.kr](mailto:thchung@dau.ac.kr)

## ABSTRACT

A diffuse and large-area dielectric barrier discharge (DBD) filled with air and helium gas mixtures was generated by a unipolar nanosecond-pulsed high voltage. A large-gap multiple pin-to-plate electrode was employed to facilitate the insertion of well plates into the plasma discharge. The nanosecond high-voltage-pulsed discharge has unique advantages in producing a diffuse DBD plasma. We examined the changes in the plasma properties upon varying operating parameters such as the gas composition and flow rate, as well as the pulse voltage. Various types of liquid (de-ionized, tap, and saline water, as well as phosphate buffered saline and LB broth) were exposed to the DBD plasma. The physicochemical properties (pH and electrical conductivity) and concentrations of reactive species generated in the treated liquids (such as  $\text{H}_2\text{O}_2$ ,  $\text{NO}_2^-$ , and  $\text{O}_3$ , which play central roles in the aqueous-phase chemistry of plasma-treated liquids for bacterial inactivation) were measured as a function of the operating parameters. The nanosecond-pulsed DBD was observed to generate significantly higher level of reactive species in various types of liquid. For investigating the plasma treatment of liquids containing suspended microorganisms, 1 ml of *Escherichia coli* (*E. coli*) stock suspension was pipetted into 9 ml of DW. The resulting bacterial suspensions were treated with the DBD plasma for a selected time. Six-log *E. coli* reduction was achieved after 19 h of incubation. A DBD plasma generated in a gas mixture of ambient air and 2 slm helium exhibited an enhanced inactivation efficacy, which was correlated with the RONS concentration and pH in the plasma-treated liquids.

Published under an exclusive license by AIP Publishing. <https://doi.org/10.1063/5.0241367>

## I. INTRODUCTION

Cold atmospheric-pressure plasmas (CAPs) have attracted huge attention because of their potential applications in surface treatment,<sup>1,2</sup> thin film deposition,<sup>3</sup> food and agriculture,<sup>4–7</sup> bacterial inactivation,<sup>8–14</sup> as well as cancer therapy.<sup>15–18</sup> Many of these applications require low-power plasmas with high chemical reactivity at low gas temperatures.<sup>19</sup> The two main groups of devices used for generating CAPs for biological and medical applications are plasma jets and dielectric barrier discharges (DBDs).<sup>17</sup> DBDs generate plasma in contact with the surface being treated.<sup>20</sup> Owing to their conventional electrode geometry, DBDs can typically provide a much larger surface area compared to plasma jets. Because of their enhanced plasma chemistry, DBDs have been widely investigated for some emerging applications, such as biological and chemical decontamination of media under ambient conditions.<sup>21</sup>

DBDs typically present a parallel-plate electrode geometry, where at least one of the electrodes is covered by a dielectric layer.<sup>22–26</sup>

Depending on the application, they have different geometries: coaxial cylindrical electrodes,<sup>27–29</sup> surface DBDs,<sup>4,8,10,30–32</sup> floating electrodes,<sup>33</sup> a sharp curved electrode combined with a flat one (point-to-plate electrode),<sup>34,35</sup> array needles to plate electrode,<sup>36–40</sup> and multiple pin-to-plate electrodes.<sup>18,41</sup> The pin electrode configuration enhances the electric field around the tip, thereby ionizing the air surrounding the pin to generate a high-intensity CAP.<sup>41</sup> The composition of the working gas plays a crucial role for the efficient operation of plasma devices. For biological applications, air,<sup>10,12,26,30,34,42</sup> argon,<sup>22,43–46</sup> or helium,<sup>47–51</sup> as well as mixtures of an inert gas with air<sup>19,25,29,45,52</sup> are commonly employed as feeding gas.

Many investigations of CAPs use alternating current (AC),<sup>1,4,12,21,48</sup> radio frequency (RF),<sup>53</sup> and submicrosecond- or microsecond-duration pulses<sup>10,30,49,54</sup> for plasma generation. Traditionally, DBDs generated via AC excitation have been widely studied for their applications.<sup>1</sup> Although DBDs can easily realize room-temperature and large-volume treatments

without gas flow (that is, in ambient air), the electron densities are usually less than  $10^{14} \text{ cm}^{-3}$ , resulting in a lower density of reactive species, which leads to a slower processing.<sup>6</sup> Recently, pulsed-excitation DBDs have been actively investigated for achieving plasmas with higher chemical efficiencies compared with those excited using an AC power supply.<sup>22,27,31</sup> The fast-rise time voltage pulse causes more electrical energy to go into the production of energetic electrons (that efficiently dissociate, excite, or ionize gases to form active species and play a crucial role in plasma-chemical processes), rather than into gas heating.<sup>22</sup> Short high-voltage pulses can be used to achieve a further increase in ionization and extend the electron energy distribution to higher values.<sup>31,47,55</sup> In this regard, nanosecond-pulsed DBDs have been shown to generate a diffuse and uniform discharge.<sup>16,34</sup> Nanosecond-pulsed plasmas can provide greater flexibility and produce a wider range of reactive species.<sup>8,15</sup> Rather than the ambient air operation, the introduction of inert gases is also known to give rise to the production of inert excited species that can bombard and interact with sample surfaces, producing more binding sites, or facilitate the formation of other reactive species, such as OH and  $\text{N}_2^*$ , through synergistic energy transfers.<sup>29</sup> Hence, to achieve uniform DBDs and highly reactive plasma generation,<sup>15,52,56</sup> in this study, we investigated a nanosecond-pulsed DBD with a helium-air mixture.

Plasma-liquid interactions has become an important topic in plasma medicine, because liquid-phase chemistry is considered the key element to understand the precise mechanisms responsible for CAP effects on living systems.<sup>57–60</sup> Plasma treatment of various types of liquid including non-buffered aqueous liquids (de-ionized water, tap water, and saline solution) and buffered solutions is of great interest for plasma medicine and agriculture. Nanosecond-pulsed DBD can be a good choice of plasma source for plasma-liquid interactions. This paper explores the competency of a large area nanosecond-pulsed DBD using multiple pin-to-plate electrodes for plasma-liquid interactions. To determine the optimal operating parameters for a specific application, measurements on physicochemical properties (pH and electrical conductivity) and concentrations of reactive species generated in the plasma-treated liquids need to be performed.

The treatment of bacteria suspended in liquids using non-thermal plasmas has been extensively studied.<sup>8,9,11,19,21</sup> CAPs applied to the surface of an aqueous solution have been shown to efficiently destroy bacteria suspended in the liquid.<sup>59</sup> It is well known that the source frequency, voltage, and power employed for CAP generation, as well as the type of device, operating gas composition, and flow rate influence the discharge properties and chemical features of CAPs,

hence, also affecting their antimicrobial efficacy.<sup>16,61</sup> In particular, the bacterial inactivation of large-area aqueous solutions is of high interest. For this purpose, there is an urgent need for further studies of different discharge configurations, such as large-area DBDs: a large-gap pin-to-plate atmospheric-pressure plasma reactor has been applied to the study of the interactions of plasma species with cell cultures.<sup>18</sup> This paper demonstrates that a multiple pin-to-plate nanosecond-pulsed DBD can effectively inactivate microorganisms in liquids both by direct plasma treatment (i.e., the microorganisms to be inactivated were present during the plasma treatment of the liquid)<sup>22,59</sup> and indirect plasma treatment, where the plasma is generated in close contact with the liquid surface and the treated liquids are then applied to microorganisms.<sup>8</sup>

This paper aims to identify an optimized condition of nanosecond-pulsed DBD configuration for efficient inactivation of bacterial suspensions. Several tests were performed on *Escherichia coli* (*E. coli*) bacterial suspensions subjected to both direct and indirect treatment via plasma-treated liquids (PTLs). In addition, we investigated the effects of different gas compositions and treatment parameters on the plasma characteristics and bacterial inactivation efficacy.

## II. PLASMA GENERATION AND CHARACTERIZATION

### A. DBD plasma generation

Figure 1(a) shows a schematic illustration of the DBD source driven by a nanosecond-pulsed unipolar high voltage, along with the details of the DBD electrode. Figure 1(b) shows the plasma plumes generated under ambient air and an air-helium mixture. The powered electrode consisted of 21 pins on a disk plate with a diameter of 90 mm. The pins, made of aluminum and having a diameter and length of 5.0 and 7.5 mm, respectively, were uniformly spaced over the plate; their tip was sharpened and rounded, and their distance from the neighboring pin along the x- and y-directions on the disk plane was 15 mm. The ground electrode consisted of a stainless-steel disk plate with a diameter of 180 mm, covered by a 2 mm-thick ceramic plate. A ceramic plate with higher dielectric constant resulted in a relatively higher electric field in the gap, also leading to a greater charge accumulation.<sup>62</sup> For bacterial inactivation experiments, the volume-DBD arrangement was adapted to Petri dishes. It was observed that placing a grounded plate under a Petri dish containing the liquid sample changed the properties of the plasma.<sup>63</sup> The irradiation distance between the pin electrode and the liquid surface was adjusted in the range of 2–12 mm to investigate the influence of the gap length.

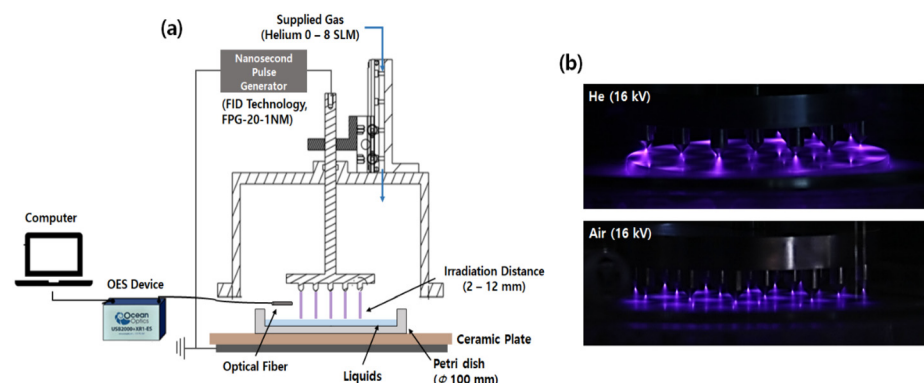


**FIG. 1.** (a) Schematic diagram of experimental setup and the details of DBD electrode. (b) The plasma plumes generated under the ambient air and air-helium mixture.

A nanosecond-pulsed DBD plasma was produced by applying a positive unipolar voltage pulse in the range of 12–18 kV between the high-voltage pin electrode and a grounded metal plate placed under the bacterial suspension containing the petri dish. The power supply (FPG-20-1 NM, FID technology) generated positive-polarity high-voltage pulses of 10 ns duration, 2 ns rise time, and 12–18 kV amplitude. The pulse repetition frequency was fixed at 360 Hz. Plasmas were generated in ambient air and in a mixture of air and helium. For air discharge, plasma was produced in ambient air without any specific gas supply. For air–helium mixture plasmas, helium was flowed into ambient air throughout the reactor at rates of 2–8 slm (standard liter per minute) through a mass flow controller (Alicat Scientific). The plume temperature was measured using a fiber-optic temperature sensor (Luxtron, M601-DM&STF) inserted into the active zone of the DBD. As shown in Fig. 2, although the plume temperature slightly increased with the applied voltage, the increase rate was rather low, and the plume temperature remained at less than 40 °C at the applied voltages of up to 18 kV. The plume temperature in an ambient air plasma was lower than that in a mixture of air and helium. The air–helium (2 slm) mixture plasma had the highest plume temperature (although the difference was not significant). An increase in the applied voltage leads to an increase in the plasma volume, which is immediately reflected by gas heating. The plume temperature depends on the plume current and on the gas flow characteristics. In ambient air plasma, the plume current is small because of insufficient gas breakdown compared to air–helium mixture. The plume temperature was observed to decrease slightly as the additive helium flow rate was further increased than 2 slm. This seems to be mainly attributed to a rise in collision frequency of hot plasma species with the surrounding molecules, effectively leading to a reduction in the plume temperature.<sup>64</sup>

When the pulse voltage was raised, the onset streamer tended to be self-sustaining and a stable thin glow appeared close to the surface of the pin electrode.<sup>25</sup> As shown in Fig. 1(b), the discharge exhibited

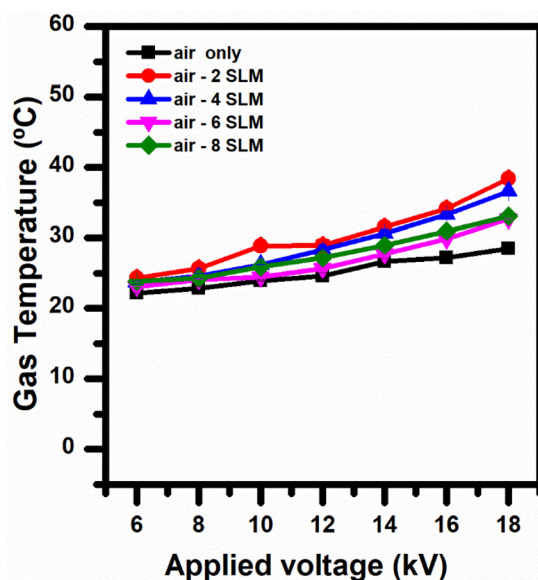


FIG. 2. Gas temperature under different gas composition (air–helium mixture) as a function of applied voltage.

the most intense discharge in the vicinity of the pin electrode and a gradual decrease in intensity with the distance from the pin electrode. However, the light intensity of the discharge becomes slightly stronger on the surface of the dielectric plate.<sup>37</sup> The stratification into dark and bright layers, typical of low-pressure glow discharges, was not observed.<sup>65</sup> With increasing helium content, the plasma emission became intense, due to the increased contribution of Penning ionization. The diffusive plasma spreads in the entire discharge gap between the electrodes. Hence, the multiple pin-to-plate electrode nanosecond-pulsed DBD ignited a large-area uniform and diffusive plasma over a relatively broad range of irradiation distances (2–12 mm) and did not heat the gas but provided strong excitation to it, due to the high energy of the electrons.

The impact of the treatment parameters on plasma-induced specific effects on the supply of reactive oxygen species (ROS) to the bottom of a liquid-filled Petri dish was investigated using a KI–starch gel reagent. This reagent, used for detecting ROS in this study, was prepared prior to being used as the target of the DBD plasma; it contained 0.3% potassium iodide, 0.5% starch, and 0.5% agarose, and was gelled by adding agarose to fix the color reactions.<sup>66</sup> Figure 3 shows that the uniformity increased with increasing treatment time, and decreased with increasing irradiation distance.

## B. Electrical characterization

Accurate voltage measurements over nanosecond times can be achieved using techniques such as back-current shunt (BCS).<sup>16</sup> For this purpose, a relatively long cable (longer than the pulse duration) was used to separate the initial pulse from the reflected pulses that oscillated between pulse generator and plasma chamber.<sup>67</sup> The pulses were delivered from the power supply to the electrodes using a 30 m-long 50-ohm high-voltage coaxial cable (RG393/U). A custom-made BCS was mounted on the cable at 15 m from the power supply to monitor the pulse shape and synchronization.<sup>56,68,69</sup> Figure 4(a) shows the  $i$ th iteration of a high-voltage pulse traveling to the load and back ( $i = 1, 2, 3$ ) in BCS measurements. We calculated the energy dissipated into plasma as the sum of the first, second, and third iterations that oscillate between the pulse generator and the load (DBD plasma).<sup>69</sup> Figure 4(b) represents high-voltage pulses propagating through the coaxial cable and measured by the BCS during the plasma experiment.

The voltage in the center wire,  $U_{HV}$ , can be written as<sup>69</sup>

$$U_{HV} = 10^{A/20} \times \frac{Z_{cable}}{R_{BCS}} \times U_{osc}, \quad (1)$$

where  $R_{BCS}$  is the total shunt resistance,  $Z_{cable}$  is the cable impedance,  $A$  is the attenuation (dB) between the oscilloscope and the BCS, and  $U_{osc}$  is the voltage applied to the port of the oscilloscope. The values employed in this study were  $R_{BCS} = 0.25 \Omega$ ,  $Z_{cable} = 50 \Omega$ , and  $A = 20$  dB. The pulse was first measured when it passed the BCS location, giving the first peak in Fig. 4, with the pulse energy designated as  $\epsilon_{1\_FWD\_BCS}$ .

$$\epsilon_{BCS} = \int_{pulse} \frac{U_{HV}^2}{50} dt. \quad (2)$$

The pulse's energy is attenuated in the coaxial cable section between the BCS and the load as it approaches the load (plasma) and

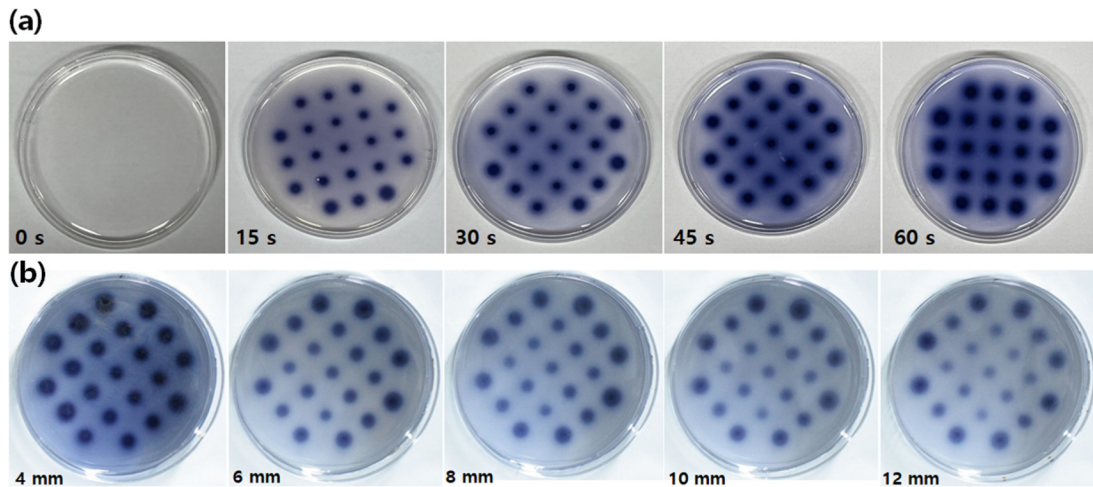


**FIG. 3.** The KI-starch gel reagent and agarose film were irradiated with the DBD plasma for (a) various treatment times and (b) irradiation distances to visualize the ROS concentration distributions.

should be accounted for as  $\varepsilon_{1_{FWD\_Load}} = \alpha^2 \times \varepsilon_{1_{FWD\_BCS}}$ , where  $\alpha$  is a unitless voltage attenuation coefficient, determined by comparing the magnitudes of the incident and reflected pulses onto the discharge cell with no plasma present ( $\alpha = 0.9$  in this experiment). Figure 4(b) shows the attenuated high-voltage pulses ( $U_{osc}$ ) propagating through the coaxial cable and measured by the BCS during the plasma experiment. A portion of the incident energy is reflected ( $\varepsilon_{1_{REV\_Load}}$ ) and transmitted back toward the BCS and pulse generator. This is measured by the BCS with energy  $\varepsilon_{1_{REV\_BCS}}$ , and yields the second peak (directed downward) in Fig. 4. Considering the cable attenuation, the original reflected pulse energy may be obtained as  $\varepsilon_{1_{REV\_Load}} = \frac{1}{\alpha^2} \times \varepsilon_{1_{REV\_BCS}}$ . Thus, we can calculate the energy deposited into the plasma as  $\varepsilon_{1_{Load}} = \varepsilon_{1_{FWD\_Load}} - \varepsilon_{1_{REV\_Load}}$ . The total amount of energy dissipated into plasma is determined, as shown in Table I. The energy per pulse was obtained as 2.5 mJ. Because the pulse repetition frequency was set as 360 Hz, the power was calculated to be 0.9 W. The energy dissipated into plasma must be calculated to compare the energy efficiency of plasma sources in achieving a certain concentration of reactive oxygen and nitrogen species (RONS), and thus realizing biological effects such as bacterial inactivation.

### C. Optical characterization

An optical spectrometer (Ocean Optics USB-2000+XR-ES) was used to quantify the relative proportions of reactive species in the DBD plasma discharge. The optical emission spectra produced by the nanosecond pulsed DBD in ambient air, air-2 slm helium, and air-4 slm helium under the condition of 10 kV pulse peak voltage and 360 Hz pulse repetition rate are illustrated in Fig. 5(a).

The spectra consisted of helium lines, atomic lines, and bands originating from gas impurities (nitrogen, oxygen, and water vapor).<sup>50</sup> The gas composition is an experimental parameter that determines the density of excited species generated by DBD. Table II selectively lists the important reactions occurring in the gas phase and plasma-liquid interface for air-helium mixture

plasmas.<sup>9,10,70</sup> The inclusion of helium resulted in a rather strong  $N_2^+$  first negative system (FNS) at 391.4 nm, due to a resonant reaction channel between metastable helium and nitrogen in the ground state. In helium plasmas, helium excited species (metastable) play a central role in the generation of electrons and  $N_2^+$  ( $B^2\Sigma_u^+$ ) states through the Penning ionization reaction (R3;  $He^m + N_2(X) \rightarrow He + N_2^+(B) + e$ ). Another reaction channel for the FNS is represented by excitation via electron collision followed by de-excitation in the ground state.<sup>50</sup> Then, the  $N_2^+$  ( $B^2\Sigma_u^+$ ) states underwent a radiative decay responsible for the FNS  $N_2^+$  emission ( $B^2\Sigma_u^+ \rightarrow X^2\Sigma_g^+$ ) at 391.4 and 426.2 nm. Conversely, in nanosecond-pulsed helium plasmas, the emission bands due to the  $N_2^+$  second positive system (SPS:  $C^3\Pi_u \rightarrow B^3\Pi_g$ ) at 315.9, 337.1, 357.7, and 380.6 nm were reduced compared to those of AC or microsecond-pulsed plasmas,<sup>2</sup> owing to most  $N_2$  being ionized. The ambient air present in the system carries a certain amount of humidity and thus of adsorbed moisture.<sup>29</sup> The appearance of OH and atomic hydrogen ( $H_\alpha$ ) peaks at 309.1 and 656.2 nm, respectively, in the spectra demonstrates the intake of some water into the gas phase, partially taking place through the plasma-liquid interface. The 777.4 nm line originates from highly reactive excited O atoms. However, in the air-only case, hydrogen ( $H_\alpha$ ), and O peaks were not shown due to a poor sensitivity of the spectrometer. The SPS and FNS bands increased slightly when 2 slm of helium was added. This may be attributed to the increase in Penning excitation and ionization. When the helium content was further increased than 2 slm, SPS and FNS bands decreased, while helium peaks increased.

It should be noted that the line intensities from triplet states at 587.6 nm ( $He: 3d^3D \rightarrow 2p^3P$ ) and singlet states at 667.8 nm ( $He: 3d^1D \rightarrow 2p^1P$ ) were very high compared to those obtained from microsecond-pulsed plasmas.<sup>2</sup> This implies that nanosecond-pulsed DBD plasmas contain a large proportion of high-energy electrons. The characteristic spectral lines of helium at 587.6, 667.8, 706.5, and 728.1 nm were selected to determine the excitation temperature ( $T_{exc}$ ) by using the Boltzmann approximation,  $\ln\left(\frac{\lambda_{pq}I_{pq}}{A_{pq}g_p}\right) = -\frac{E_p}{kT_{exc}} + const$ ,

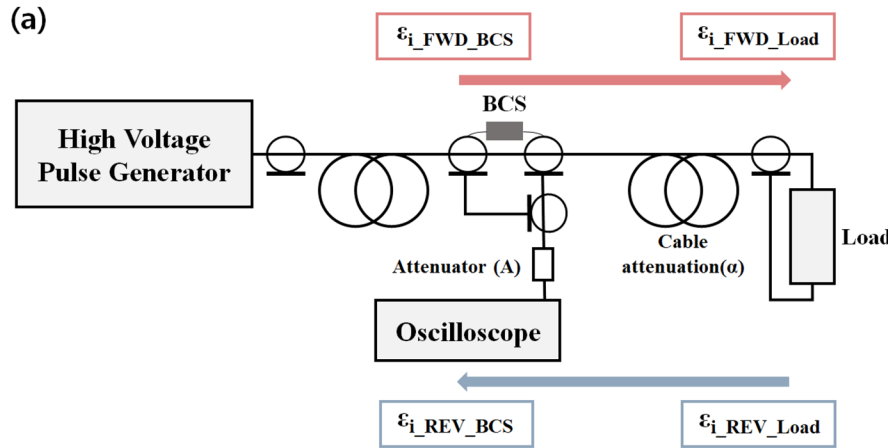
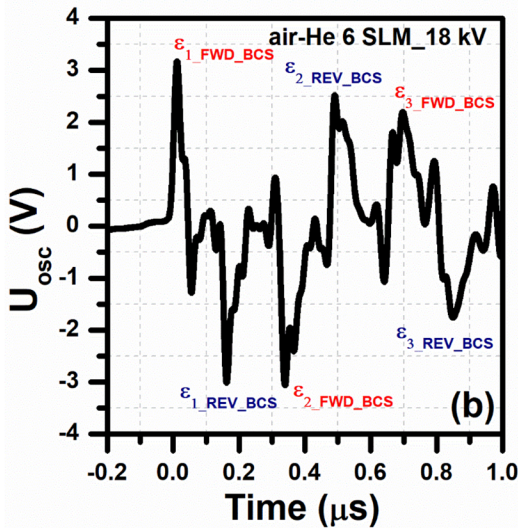


FIG. 4. (a) The scheme of typical BCS measurements shows the  $i$ th iteration of a HV pulse traveling to the load and back ( $i=1, 2, 3$ ). (b) Attenuated high-voltage pulses ( $U_{osc}$ ) propagating through the coaxial cable and measured by the BCS (back current shunt) during plasma experiment.



where  $\lambda_{pq}$ ,  $I_{pq}$ , and  $A_{pq}$  are the wavelength, intensity, and Einstein coefficient of the transition line, respectively, and  $E_p$  and  $g_p$  represent the energy and degeneracy of the upper level, respectively. Figure 5(b) illustrates the excitation temperature as a function of the flow rate of added helium.  $T_{exc}$  was 0.44 eV at air-2 slm helium and exhibited a slight decrease with increasing helium content. A collisional-radiative model based on pure helium discharge predicts that the electron temperature can be deduced from the analysis of the intensity ratio between the triplet states at 587.6 nm ( $3d\ ^3D \rightarrow 2p\ ^3P$ ) and 706.5 nm ( $3s\ ^3S \rightarrow 2p\ ^3P$ ), which are solely dependent on the electron temperature.<sup>71</sup> Figure 5(c) illustrates the emission intensity ratio of He (587.6 nm) to He (706.5 nm) as a function of the flow rate of added helium. The intensity ratio exhibited a slight decrease with increasing helium content and the estimated electron temperature were relatively high (around 0.6–1.0 eV). The variations in line intensity ratio of He (587.6 nm) to He (706.5 nm) showed a similar trend to the excitation temperature.

### III. PLASMA TREATMENT OF LIQUIDS

#### A. Reactive species generation

$H_2O_2$ ,  $NO_2^-$ , and  $O_3$  are among the main RONS in atmospheric-pressure plasma in contact with water, and play central roles in the aqueous-phase chemistry of plasma-treated liquid media for bacterial inactivation.<sup>26,48</sup> In plasma discharges, highly excited  $N_2$  reacts with atomic O, producing NO and atomic N species in the gaseous phase ( $R19; O + N_2^* (^1\Sigma_g^+, v) \rightarrow NO + N$ ); then, atomic N becomes a source of NO via the reaction with  $O_2$  gas ( $R21; N + O_2 \rightarrow NO + O$ ). Atomic O, mainly generated from electron dissociation of oxygen molecules (R7), produces strong oxidants, such as  $O_3$  (R24) or OH (R13). Gas-phase  $O_3$  is mainly formed by a three-body reaction (R24). These oxidants react with NO, producing nitrogen oxides ( $N_xO_y(g)$ ). Gaseous nitrous acids ( $HNO_3(g)$ ) are formed by  $N_xO_y(g)$  (R27, R32), which reacts with  $H_2O$  vapor ( $R30; N_2O_3(g) + H_2O(g) \rightarrow 2HNO_3(g)$ ), and are then dissolved into the liquid (R31, 34;

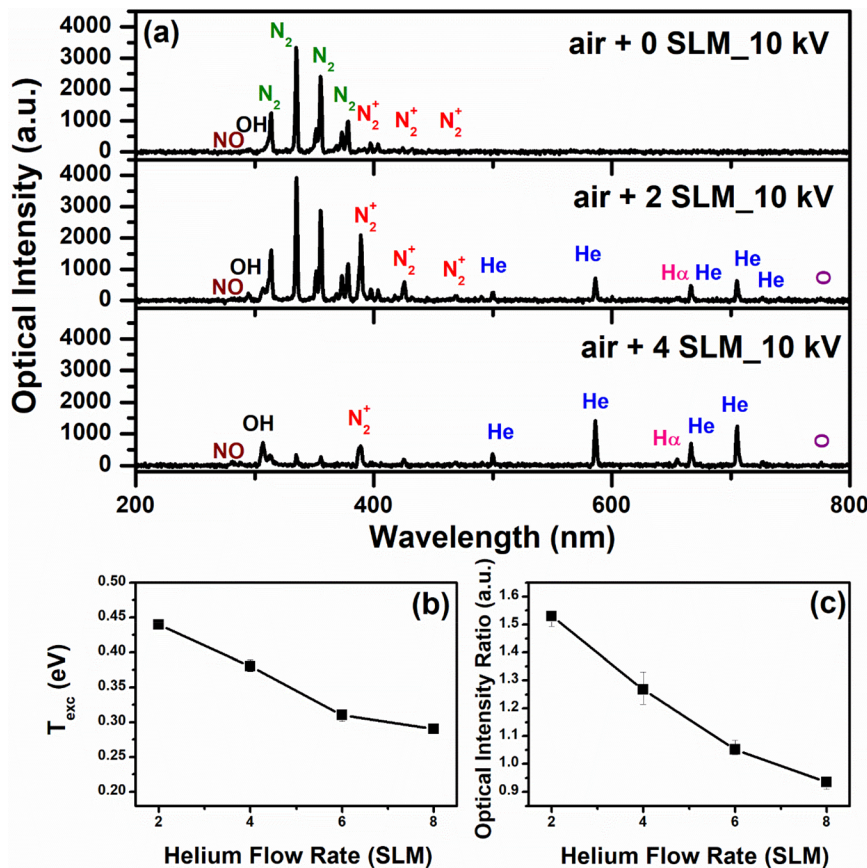


FIG. 5. (a) Optical emission spectra for the plasmas generated in air–helium mixtures (0, 2, and 4 slm helium) under the condition of 10 kV pulse peak voltage and 360 Hz pulse repetition rate. (b) The excitation temperature estimated based on the Boltzmann plot and (c) the intensity ratio of atomic lines He (587.6 nm)/He (706.5 nm) as a function of the helium content.

$\text{HNO}_x(\text{g}) \rightarrow \text{HNO}_x(\text{aq})$ ). The direct bactericidal effect of  $\text{NO}_2^-$  species under acidic conditions is well known.<sup>9,12</sup> The  $\text{H}_2\text{O}_2$  generation pathway is mainly based on the electron-impact dissociation of  $\text{H}_2\text{O}$  (R10;  $\text{H}_2\text{O} + e \rightarrow \text{OH}^* + \text{H} + e$ ). The resulting  $\text{OH}^*$  species can directly dissolve in the liquid or combine in the gaseous phase (R18).  $\text{OH}^*$  species dissolved in the liquid also combine to form hydrogen peroxide ( $\text{H}_2\text{O}_2$ ).<sup>70</sup> The latter is a biologically active agent known for its significant antimicrobial and cytotoxic properties in PTLs. Moreover,  $\text{H}_2\text{O}_2$  can intensify the cytotoxic effect of  $\text{NO}_2^-$  species in an acidic environment.<sup>9</sup>

DBD-produced ozone has been used in many applications such as sterilization, purification, and oxidation due to its strong chemical reactivity. Therefore, the ozone generation serves as a good measure

for the assessment of DBD reactors.<sup>28</sup> In particular, ozone ( $\text{O}_3$ ) is known to contribute to the bactericidal effects even under non-acidic conditions.<sup>72</sup> The peroxone chemistry between ozone and hydrogen peroxide generates additional OH radicals ( $\text{R29}; \text{H}_2\text{O}_2 + \text{O}_3 + \text{OH}^- \rightarrow \text{OH}^* + \text{HO}_2 + \text{O}_2 + \text{OH}^-$ ). The reactive species and ions formed in PTLs result in an acidic pH and increased electrical conductivity.<sup>7,73</sup>

The concentrations of long-lived reactive species such as  $\text{H}_2\text{O}_2$  and  $\text{O}_3$  in the PTL were determined spectrophotometrically using a PhotoLab 7600 instrument (WTW, Germany), according to the instructions provided by the manufacturer. The nitrite ( $\text{NO}_2^-$ ) concentration was determined using the Griess reagent (Molecular Probes). The electrical conductivity and pH of de-ionized water (DW) were measured with an Ohaus Starter ST3100C conductivity meter

TABLE I. Calculation of energy deposited into the plasma.

Iteration	Forward energy (mJ)		Reverse energy (mJ)		Energy deposited into the plasma
	BCS location	Load location	BCS location	Load location	
First	17.1	13.86	10.6	13.09	0.77
Second	25.1	20.33	15.6	19.3	1.03
Third	18.4	14.9	11.5	14.2	0.7
Total $\epsilon_{load}$ (mJ)					2.5

TABLE II. Set of the most important reactions involved in the gas phase and plasma–liquid interface.

$\text{He} + e \rightarrow \text{He}^+ + 2e$	(R1)	$\text{N}_2 + \text{O} \rightarrow \text{NO} + \text{N}$	(R19)
$\text{He} + e \rightarrow \text{He}^* + e$	(R2)	$\text{N}_2^* + \text{O}_2 \rightarrow \text{N}_2 + 2\text{O}$	(R20)
$\text{He}^* + \text{N}_2 \rightarrow \text{N}_2^+ + \text{He} + e$	(R3)	$\text{N}(^2\text{D}) + \text{O}_2 \rightarrow \text{NO} + \text{O}$	(R21)
$\text{He}^* + \text{O}_2 \rightarrow \text{O}_2^+ + \text{He} + e$	(R4)	$\text{NO} + \text{O}_2(\text{O}_3) \rightarrow \text{NO}_2 + \text{O}(\text{O}_2)$	(R22)
$e + \text{N}_2(\text{X}) \rightarrow \text{N}_2^*(\text{A, B, C}) + e$	(R5)	$\text{NO} + \text{NO}_2 \rightarrow \text{N}_2\text{O}_3$	(R23)
$e + \text{N}_2(\text{X}) \rightarrow \text{N}_2^+(\text{X}) + 2e$	(R6)	$\text{O}_2 + \text{O} + \text{M} \rightarrow \text{O}_3 + \text{M}$	(R24)
$e + \text{O}_2 \rightarrow 2\text{O} + e$	(R7)	$\text{O}_3 + \text{O} \rightarrow 2\text{O}_2$	(R25)
$e + \text{O}_2 \rightarrow \text{O} + \text{O}^-$	(R8)	$\text{NO} + \text{OH} \rightarrow \text{HNO}_2$	(R26)
$e + 2\text{O}_2 \rightarrow \text{O}_2^- + \text{O}_2$	(R9)	$\text{NO}_2 + \text{OH} \rightarrow \text{HNO}_3$	(R27)
$e + \text{H}_2\text{O} \rightarrow \text{OH}^* + \text{H} + e$	(R10)	$\text{HNO}_2 + \text{OH} \rightarrow \text{H}_2\text{O}_2 + \text{NO}_2$	(R28)
$e + \text{H}_2\text{O} \rightarrow \text{H}^- + \text{OH}$	(R11)	$\text{H}_2\text{O}_2 + \text{O}_3 + \text{OH}^- \rightarrow \text{OH}^* + \text{HO}_2 + \text{O}_2 + \text{OH}^-$	(R29)
$\text{H}_2\text{O}^* \rightarrow \text{H}^+ + \text{OH}^-$	(R12)	$\text{N}_2\text{O}_3(\text{g}) + \text{H}_2\text{O} \rightarrow 2\text{HNO}_2(\text{g})$	(R30)
$\text{O}(^1\text{D}) + \text{H}_2\text{O} \rightarrow 2\text{OH}$	(R13)	$\text{HNO}_2(\text{g}) \rightarrow \text{HNO}_2(\text{aq})$	(R31)
$\text{H} + \text{O}_2 + \text{M} \rightarrow \text{HO}_2 + \text{M}$	(R14)	$2\text{NO}_2 + \text{H}_2\text{O} \rightarrow \text{HNO}_2 + \text{HNO}_3$	(R32)
$\text{H} + \text{HO}_2 \rightarrow 2\text{OH}$	(R15)	$\text{N}_2\text{O}_3 + \text{H}_2\text{O} \rightarrow 2\text{HNO}_2$	(R33)
$\text{N}_2(\text{A}) + \text{H}_2\text{O} \rightarrow \text{N}_2 + \text{OH} + \text{H}$	(R16)	$\text{HNO}_3(\text{g}) \rightarrow \text{HNO}_3(\text{aq})$	(R34)
$e + \text{H}_2\text{O}^+ \rightarrow \text{H} + \text{OH}$	(R17)		
$\text{OH} + \text{OH} \rightarrow \text{H}_2\text{O}_2$	(R18)		

and an Ohaus Starter ST3100 digital pH-meter, respectively. In addition to DW, various types of liquids (tap water, saline solution, phosphate buffered saline (PBS), and LB broth) were exposed to the DBD plasma, and their properties (pH and electrical conductivity) and concentrations of the generated reactive species were measured as a function of the operating parameters.

In this study, the concentration of these species in plasma-treated DW (PT-DW) were obtained as a function of the applied voltage, the gas flow of helium into ambient air, the irradiation distance, and the volume of DW. The generation of  $\text{H}_2\text{O}_2$  in liquids is influenced by the electron density and the concentrations of nitrogen, oxygen, and water vapor above the gas–liquid interface. The concentration of nitrogen and oxygen (i.e., the air concentration) above the gas–liquid interface has a significant influence on the generation of  $\text{H}_2\text{O}_2$ ,  $\text{NO}_2^-$ , and  $\text{O}_3$  in PTLs, and changes with the exposed liquid surface, the irradiation distance, and the gas composition. The air concentration is higher when using a larger exposed liquid surface and a lower helium flow rate. In particular, a larger exposed liquid surface corresponds to a higher concentration of water vapor. When the irradiation distance is longer, more helium diffuses into air during transport, thus reducing the convection of water vapor. As a result, the evaporation of water and thus the concentration of water vapor above the gas–liquid interface are reduced at a longer distance between the pin electrode and the liquid surface.

Figure 6 presents the measurements of the  $[\text{H}_2\text{O}_2]$ ,  $[\text{NO}_2^-]$ , and  $[\text{O}_3]$  performed as functions of (a) applied voltage (12–18 kV; liquid volume 10 ml; air–4 slm helium; irradiation distance 3 mm) (b) gas composition (air, air–2 slm, air–4 slm, air–6 slm, air–8 slm helium; 18 kV; 10 ml; 3 mm) (c) irradiation distance (3–11 mm; air–4 slm helium; 16 kV; 10 ml), and (d) liquid volume (10–25 ml; air–4 slm helium; 14 kV; 7 mm). The treatment time is set as 1 min for all cases. Figure 6(a) illustrated that  $[\text{H}_2\text{O}_2]$ ,  $[\text{NO}_2^-]$  and  $[\text{O}_3]$  increased with the applied voltage, as expected. This implies that these concentrations in the gas phase increased with the applied voltage and power

consumption. Notably, limited decomposition of these species was observed at high temperature, because the gas temperature increased very smoothly with the applied voltage (Fig. 2), thus, making the generation of RONS greater than the corresponding loss.

Figure 6(b) shows the changes in the  $[\text{H}_2\text{O}_2]$ ,  $[\text{NO}_2^-]$ , and  $[\text{O}_3]$  values with the gas composition. The ambient air-only case (0 slm helium) resulted in a quite low level of RONS generation because the air breakdown was not sufficient to generate enough reactive species in the gas phase. When 2 slm of helium was added to ambient air,  $[\text{H}_2\text{O}_2]$ ,  $[\text{NO}_2^-]$ , and  $[\text{O}_3]$  reached their highest values. The addition of a small amount of helium to ambient air can promote the plasma generation, thereby enhancing the excitation and ionization of neutral particles in the gas phase. However, a further addition of helium reduces the electron energy (as shown in Fig. 5), thereby suppressing the excitation and ionization of neutral particles (the sources of the reactive species were discussed earlier). Figure 6(c) shows the  $[\text{H}_2\text{O}_2]$ ,  $[\text{NO}_2^-]$ , and  $[\text{O}_3]$  changes with the irradiation distance. A longer irradiation distance corresponds to a larger gap, resulting in a weak electric field between the electrodes; this suppresses the plasma generation (and thus, the excitation and ionization of neutral particles). Reduced amounts of reactive species in the gas phase result in a decreased RONS concentration in the treated liquids.

Figure 6(d) shows measured  $[\text{H}_2\text{O}_2]$ ,  $[\text{NO}_2^-]$ , and  $[\text{O}_3]$  values as a function of the liquid volume. The figure demonstrated that smaller volumes were associated with slightly higher  $[\text{H}_2\text{O}_2]$ ,  $[\text{NO}_2^-]$ , and  $[\text{O}_3]$  levels. These relationships suggest that the species responsible for the changes in  $[\text{H}_2\text{O}_2]$ ,  $[\text{NO}_2^-]$ , and  $[\text{O}_3]$  are only formed at the plasma–liquid interface and then transferred into the liquid, and that the production rate of these species is independent of the treated volume.<sup>73,74</sup> Therefore, smaller liquid volumes result in a slight increase in the  $[\text{H}_2\text{O}_2]$ ,  $[\text{NO}_2^-]$ , and  $[\text{O}_3]$  levels.

It should be noted that the nanosecond-pulsed plasma-treated DW has a higher ozone concentration compared to those treated by AC and/or microsecond-pulsed plasmas.<sup>2</sup> Moreover, the energy

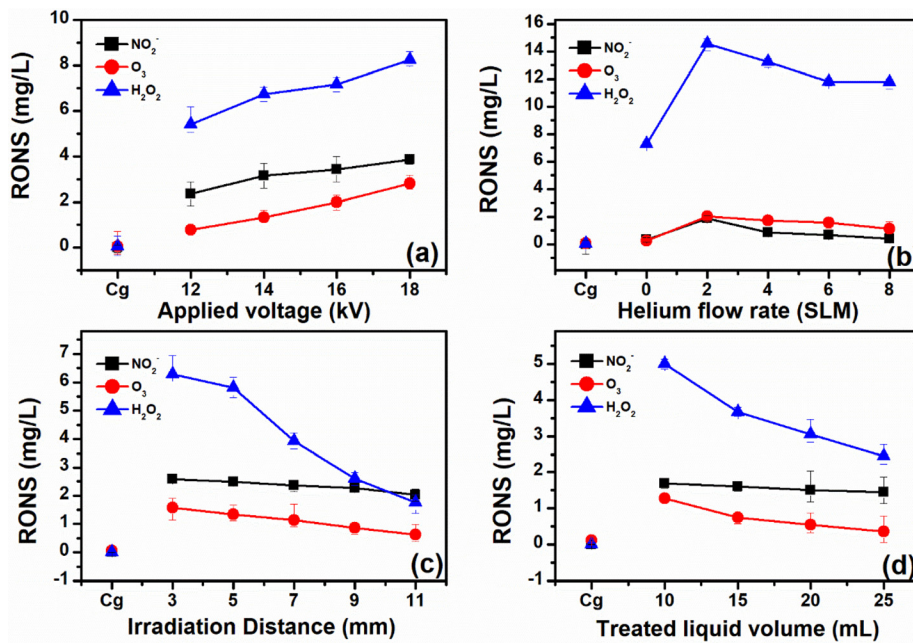


FIG. 6. Typical trend of change of long-lived RONS in DW as functions of (a) applied voltage (12–18 kV; liquid volume 10 ml; air–4 slm helium; irradiation distance 3 mm), (b) gas composition (air, air–2 slm, air–4 slm, air–6 slm, air–8 slm helium; 18 kV; 10 ml; 3 mm), (c) irradiation distance (3–11 mm; air–4 slm helium; 16 kV; 10 ml), and (d) liquid volume (10–25 ml; air–4 slm helium; 14 kV; 7 mm). Here, the treatment time is 1 min.

consumption per ozone molecule under pulse excitation was found to be lower than that measured under sine wave excitation.<sup>54</sup> The ozone production efficiency of high voltage nanosecond-pulsed DBD is attributed to the moderate gas temperature (seen in Fig. 2) as well as the quality of electrons in terms of electron density and energy.<sup>28</sup> Higher density and energy electrons generated by high voltage nanosecond-pulsed DBD enhances the electron-impact dissociation of  $\text{O}_2$  molecule (R7). Moderate (or low) gas temperature enhances the three-body formation of  $\text{O}_3$  (R24), while oppresses the recombination of  $\text{O}_3$  and O (R25). The generated ozone in gas phase is transferred into the liquid.

### B. Physicochemical properties of plasma-treated liquids

Operating parameters will affect the physicochemical properties of the plasma-treated liquids. In Fig. 7, typical trend of change of pH and electrical conductivity in PT-DW was displayed as functions of (a) applied voltage (12–18 kV; liquid volume 10 ml; air–4 slm helium; irradiation distance 3 mm) (b) gas composition (air, air–2 slm, air–4 slm, air–6 slm, air–8 slm helium; 18 kV; 10 ml; 3 mm) (c) irradiation distance (3–11 mm; air–4 slm helium; 16 kV; 10 ml), and (d) liquid volume (10–25 ml; air–4 slm helium; 14 kV; 7 mm). The treatment time is set as 1 min for all cases. A decrease in pH and increase in electrical

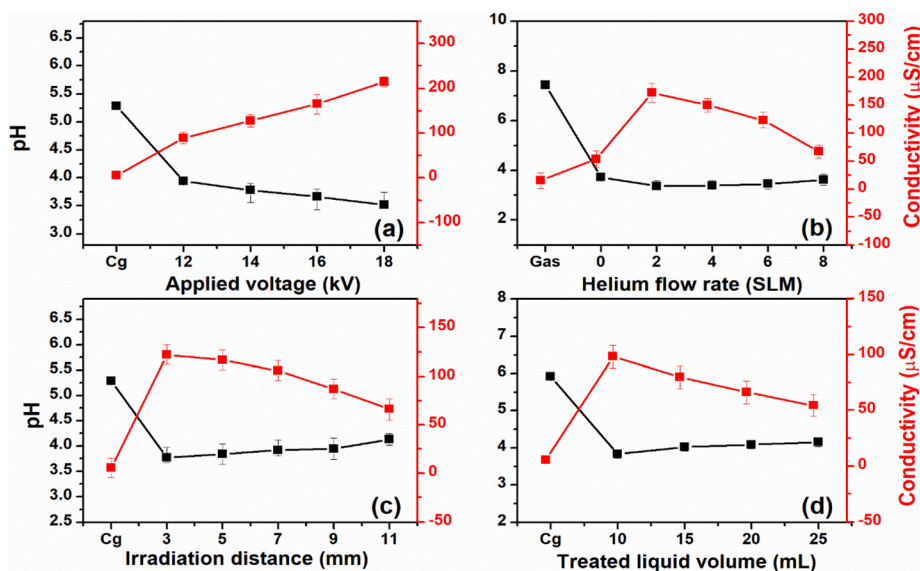


FIG. 7. Typical trend of change of pH and electrical conductivity in DW as functions of (a) applied voltage (12–18 kV; liquid volume 10 ml; air–4 slm helium; irradiation distance 3 mm), (b) gas composition (air, air–2 slm, air–4 slm, air–6 slm, air–8 slm helium; 18 kV; 10 ml; 3 mm), (c) irradiation distance (3–11 mm; air–4 slm helium; 16 kV; 10 ml), and (d) liquid volume (10–25 ml; air–4 slm helium; 14 kV; 7 mm). Here, the treatment time is 1 min.

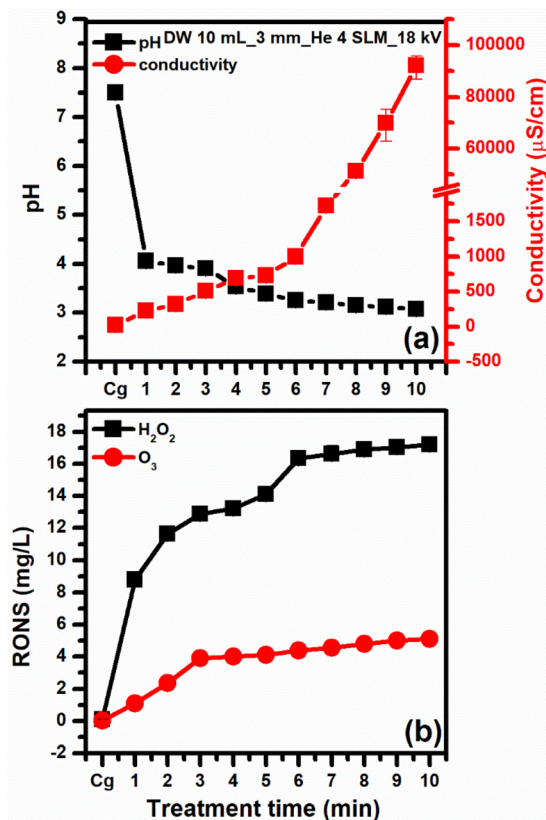


FIG. 8. (a) The pH and electrical conductivity and (b)  $[\text{H}_2\text{O}_2]$  and  $[\text{O}_3]$  in PT-DW are dependent on plasma treatment time (1–10 min). Experimental condition: DW volume 10 ml; air–helium 4 slm; applied voltage 18 kV; irradiation distance 3 mm.

conductivity were observed with an increase in applied voltage [Fig. 7(a)]. Figure 7(b) shows the changes in the pH and conductivity of the PTLs with the gas composition. When 2 slm of helium was added to ambient air, the pH reached the minimum (and the conductivity reached the maximum). This behavior is related to the concentration of reactive ions, as discussed above. The dependences of pH and electrical conductivity on irradiation distance and liquid volume were consistent with those of RONS concentrations shown in Fig. 6 [Figs. 7(c) and 7(d)].

Figure 8 presents the changes in pH and conductivity of the PT-DW with the treatment time. Measurement was performed at a specific condition (DW volume 10 ml; air–helium 4 slm; applied voltage 18 kV; irradiation distance 3 mm). The pH showed a substantial drop in the first minute of treatment. In the next 10 min, the pH continued to decrease until stabilizing at around 3 after 10 min. The electrical conductivity of the PTL increased almost linearly with the plasma treatment time; the increase rate became higher from 6 min of treatment onward, and the conductivity reached 9000  $\mu\text{S}/\text{cm}$  after 10 min of treatment.<sup>11</sup> This drastic increase may be related to the cumulative effect of plasma–liquid interactions. Surfaces in contact with plasma are exposed to plasma-generated reactive species, ions/electrons, and UV radiation, resulting in surface charging, photoionization, secondary electron emission, de-excitation, and radical reactions at the

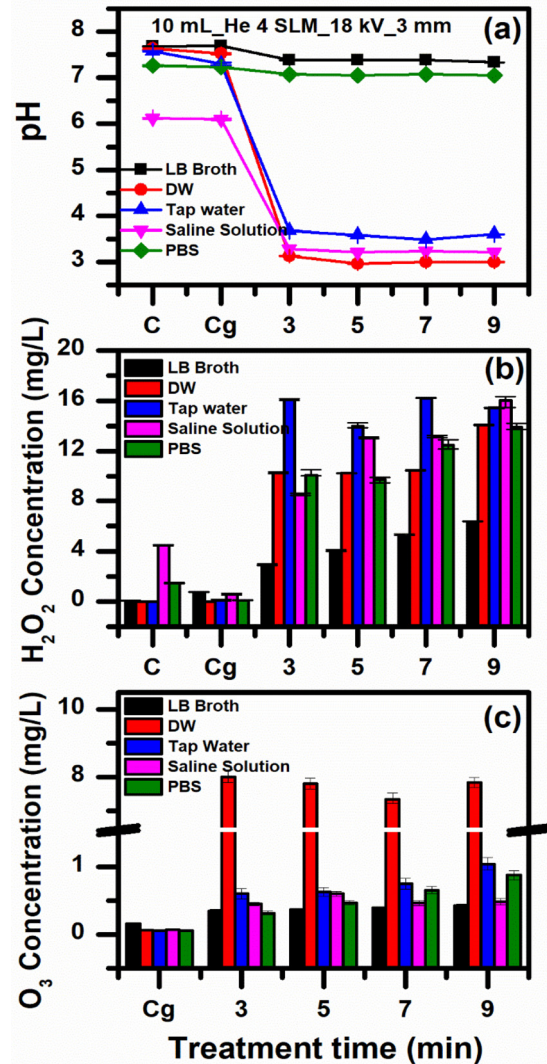
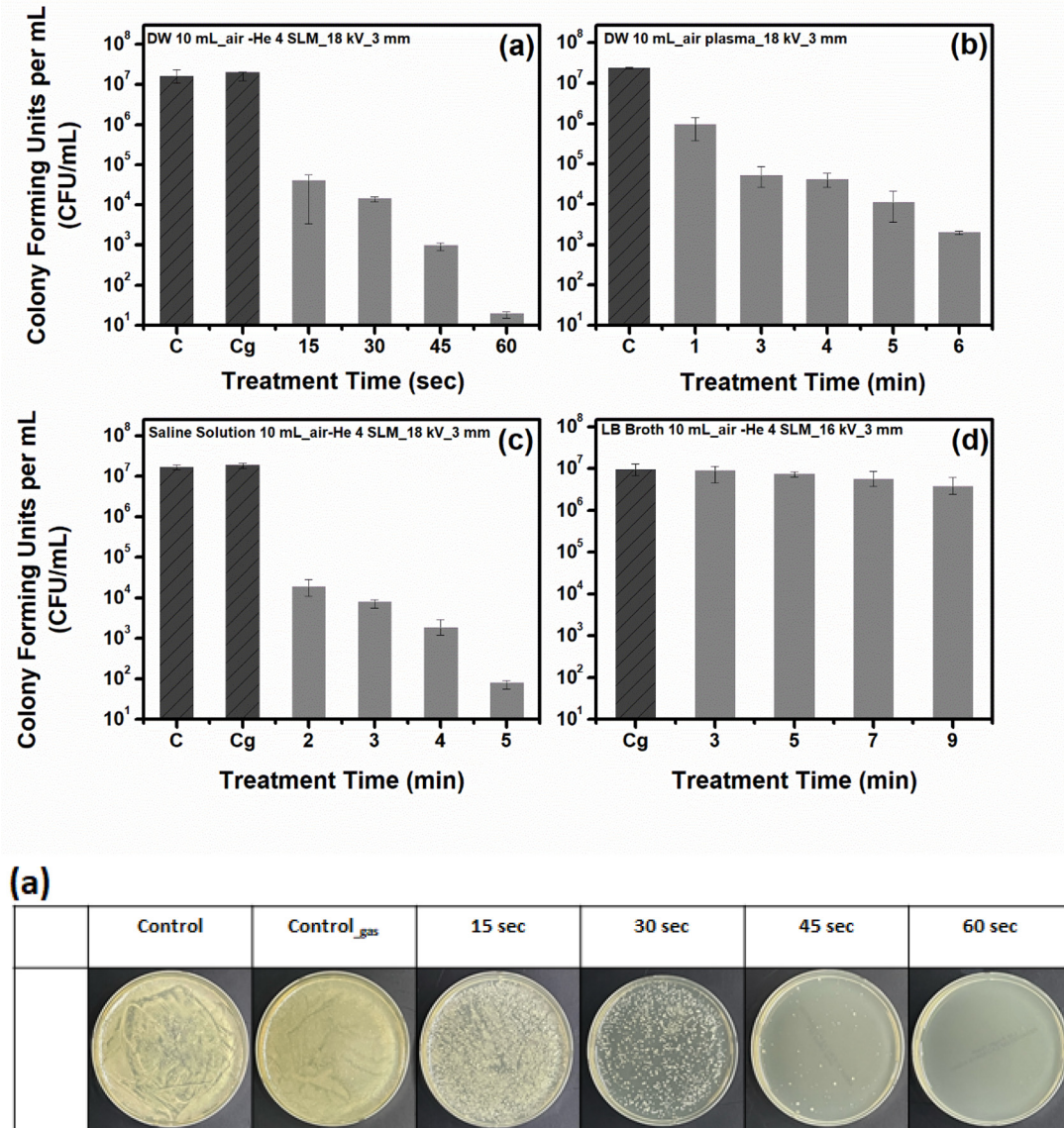


FIG. 9. The pH in different plasma-treated media (LB broth, DW, tap water, saline solution, and PBS) for various treatment time (3–9 min). (b)  $[\text{H}_2\text{O}_2]$  and (c)  $[\text{O}_3]$  in different treated media as a function of plasma treatment time (1–10 min). Experimental condition: liquid volume 10 ml; air–helium 4 slm; applied voltage 18 kV; irradiation distance 3 mm.

surfaces. The physical properties of the sample, such as conductivity, permittivity, surface roughness, and surface energy, establish the boundary conditions for the distribution of electric fields, determining sheath formation. In turn, this impacts discharge initiation and propagation, and thus the energy in the plasma and the flux of ions, electrons, and reactive species to the surface.<sup>62</sup>

Electrical conductivity measurements can confirm the amounts of active ions present in PTLs.<sup>11</sup> As discussed above, gas-phase RONS are transferred into the liquid phase. The conductivity of the treated water is mainly due to positive  $\text{H}^+$  as well as negative  $\text{NO}_2^-$  and  $\text{NO}_3^-$  ions;<sup>59,73,75</sup> these species are also responsible for the pH drop. Oehmigen *et al.* reported that the main cause for the acidification of plasma-treated water is the formation of  $\text{H}^+$  and  $\text{HNO}_3^-$  ions.<sup>9</sup> Vlad



**FIG. 10.** Bactericidal effect on *E. coli* as a function of treatment time for direct treatment on bacterial suspension: (a) in DW under air–4 slm helium (applied voltage 18 kV) during 45 s, (b) in DW during 6 min under air plasma (18 kV), (c) in saline solution under air–4 slm helium (18 kV) during 5 min, and (d) in LB broth under air–4 slm helium (16 kV) during 9 min. Here, the irradiation distance is 3 mm for all the cases. The corresponding photographs of bacterial samples on agar plates for (a) are shown. The control group is also presented.

and Anghel suggested that the acidification and electrical conductivity increase in plasma-treated liquids are due to the formation of  $\text{NO}_3^-$ / $\text{HNO}_3$  species.<sup>73</sup>

We also examined different plasma-treated solutions (non-buffered and buffered solutions). The experiments were performed at a specific condition (liquid volume 10 ml; air–helium 4 slm; applied voltage 18 kV; irradiation distance 3 mm). Figure 9(a) shows the pH changes with the treatment time for various types of liquids. The plasma treatment of non-buffered aqueous liquids (DW, tap water, and saline solution) resulted in a pH decrease, caused by nitric and nitrous acids.<sup>9</sup> Conversely, the buffered solutions (PBS and LB broth)

did not exhibit a significant change in pH. Deionized water, tap water, and saline solution exhibited a similar decreasing trend with increasing treatment time. Strong acidification of PTLs is typically observed for nonbuffered media such as saline solution and DW. The pH values were saturated after 3 min of treatment, and decreased in the order DW > saline solution > tap water. As was observed in an earlier study by Oehmigen *et al.*,<sup>9</sup> the difference of pH between DW and saline solution is insignificant. As mentioned earlier, the pH decrease is due to the formation of acids like  $\text{HNO}_3$  and  $\text{HNO}_2$ . However, the concentration of these acids may depend on various factors like concentration of the excited species formed and their transformation to mineral acids.<sup>76</sup>

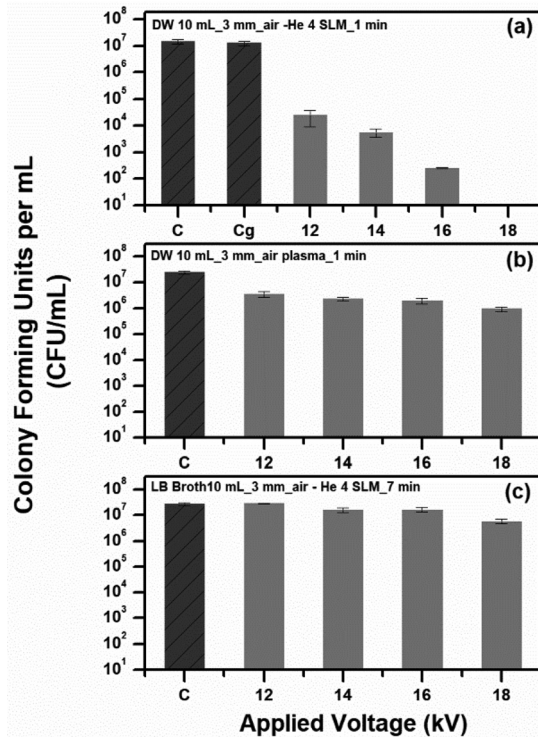


**FIG. 11.** Bactericidal effect on *E. coli* as a function of applied voltage for direct treatment on bacterial suspension: (a) in DW after 1 min under air-4 slm helium, (b) in DW after 1 min under air plasma, and (c) in LB broth after 7 min under air-4 slm helium. Here, the irradiation distance is 3 mm for all the cases.

In saline solution and tap water, the chlorine compounds (HOCl, OCl<sup>-</sup>, ClO<sub>2</sub>, ClO<sub>3</sub>, NaOCl, and NH<sub>2</sub>Cl) following the reactions of RONS with Cl<sup>-</sup> may influence these factors.<sup>77</sup> In general, the pH value is considered a critical parameter for bacterial inactivation.<sup>59,72</sup>

Figures 9(b) and 9(c) show the H<sub>2</sub>O<sub>2</sub> and O<sub>3</sub> concentrations in different PT media as a function of the treatment time. The different types of media contained rather high [H<sub>2</sub>O<sub>2</sub>] levels, except for LB broth. This implies that the plasma-activated media prepared by nanosecond-pulsed DBD can be effectively employed for cancer therapy.<sup>15,18,60</sup> Conversely, PT-DW had the highest [O<sub>3</sub>] level, which was significantly larger compared to the other media. The nanosecond-pulsed DBD produced much higher H<sub>2</sub>O<sub>2</sub> and O<sub>3</sub> concentrations with a larger liquid volume compared to those generated by low-frequency or microsecond-pulsed plasmas.<sup>2</sup>

#### IV. BACTERIAL INACTIVATION EXPERIMENTS

Infectious microorganisms are usually found in a wet and nutrient-rich environment; therefore, they have to be inactivated under these conditions, which are optimal for growth and infection progression. The inactivation of microorganisms has been frequently investigated using *in vitro* models mainly based on half-rigid nutrient media (agar) plates, which are useful to simulate nutrient-rich as well as wet and thus optimal living conditions for bacteria.<sup>78</sup> The inactivation efficiency of the DBD device was tested by treating *Escherichia coli*

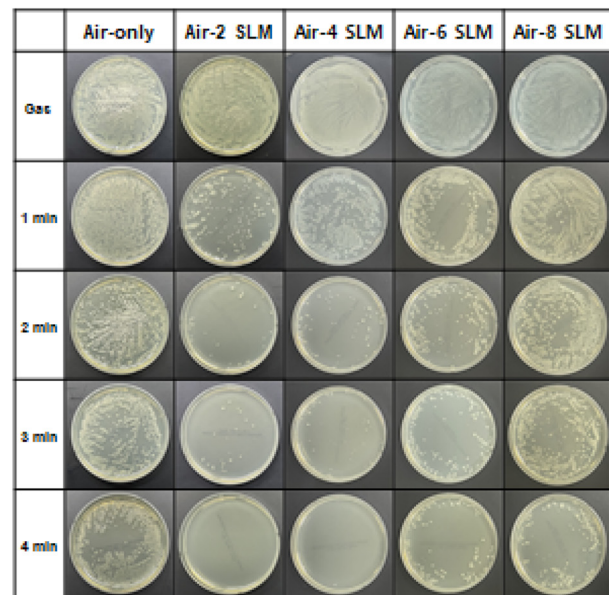
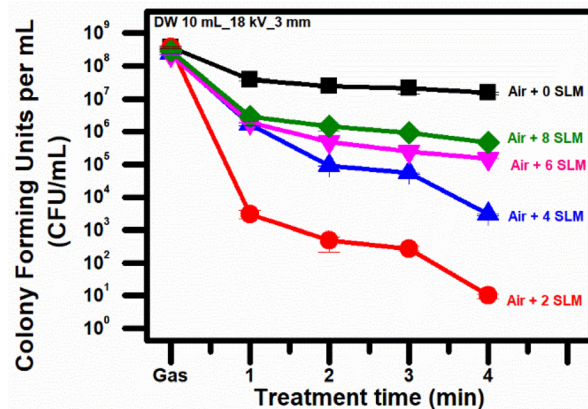


**FIG. 12.** Survival curve of *E. coli* under the direct treatment for different helium contents in ambient air (18 kV). Here, the irradiation distance is 3 mm for all the cases. The corresponding photographs of bacterial samples on agar plates are shown.

(*E. coli*) bacteria in distilled water and counting the number of surviving colony-forming units (CFUs).

*E. coli* bacteria (initial concentration  $\sim 3 \times 10^8$  CFU/ml), provided by Professor Sun Hee Leem (Laboratory of Cancer Genomics, Dong-A University), were diluted using LB culture media to achieve concentrations of  $10^5$ – $10^8$  CFU/ml. The initial concentrations were verified by triplicate dilution plate counts (in sterile de-ionized water) on LB agar. For the plasma treatment of liquids containing suspended inoculum, 1 ml of *E. coli* suspension was pipetted into 9 ml of DW (or LB broth). The resulting bacterial suspensions were treated with the DBD plasma for different times (1–10 min). After treatment for a selected time, 0.5 ml of the treated bacterial suspensions was diluted by the serial dilution method with DW to an appropriate density, and spread-plated onto LB agar culture medium in a standard Petri dish, which was then incubated at 37 °C for 19 h for measuring the CFU

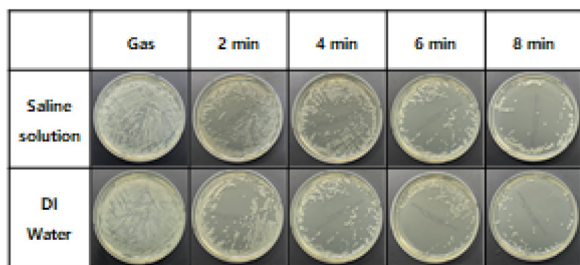
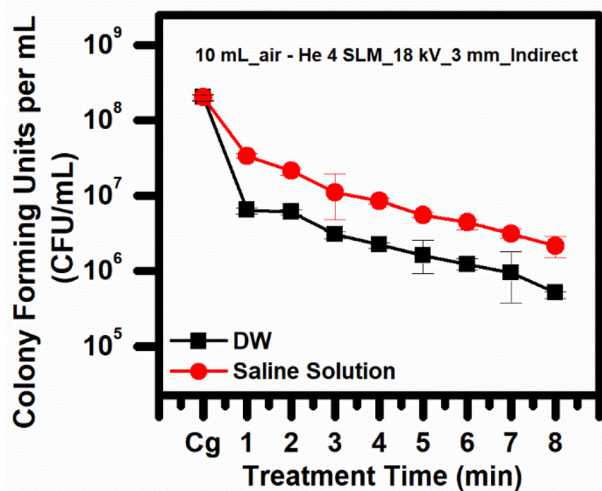


**FIG. 13.** Comparison of bactericidal effect on *E. coli* under the indirect treatment between PT- DW and PT- saline solution as a function of treatment time during 8 min. Experimental condition: liquid volume 10 ml; air–helium 4 slm; applied voltage 18 kV; irradiation distance 3 mm. The corresponding photographs of bacterial samples on agar plates are shown.

counts (surface-spread plate count method). Then, we calculated cell colony counts and bacteria reduction rates. All experiments were repeated three times.

For the indirect treatment, 10 ml of de-ionized water was placed in the same dishes; after the plasma treatment for a prescribed time, 1–3 ml of the initial bacteria was introduced into a portion of the treated de-ionized water to prepare a fixed volume (10 ml) of bacterial suspension. The surviving bacteria were counted by the plate dilution method to determine the inactivation efficiency.

We measured the inactivation efficacy of DBD systems with different operating parameters, such as applied voltage, gas composition, treatment time, and media type supporting *E. coli*. The inactivation system exhibited a reduction in the colony count with increasing treatment time. Figure 10 shows the reduction of the *E. coli* content under direct treatments. Direct treatment of *E. coli* suspended in DW by DBD in a gas mixture of air–4 slm helium (applied voltage: 18 kV, irradiation distance: 3 mm) resulted in a 6-log reduction within 1 min [Fig. 10(a)]. Treatment in tap water under the same operating conditions achieved a complete inactivation of *E. coli* within 2 min (not shown in the figure). Furthermore, the same direct treatment of *E. coli* suspended in saline solution under the same operating conditions

resulted in a 5-log reduction within 5 min [Fig. 10(c)]. Conversely, the same direct treatment of *E. coli* suspended in DW by DBD operated in ambient air under the same applied voltage and irradiation distance achieved a 4-log CFU reduction of *E. coli* in 6 min [Fig. 10(b)]. However, as a consequence of the non-acidic environment, the bactericidal effect in LB broth in a gas mixture of air–4 slm helium (applied voltage: 18 kV, irradiation distance 3 mm) was strongly reduced compared to that in non-buffered solutions [Fig. 10(d)].<sup>48,72</sup> The corresponding photographs of bacterial samples on agar plates for (a) are shown. With a proper dilution, the CFU for the control group was counted by the surface-spread plate count method.

Next, we explored the effect of the applied voltage on the inactivation efficacy of the DBD system. As expected, the inactivation efficacy increased with the applied voltage (Fig. 11). This behavior was observed regardless of the supporting media (DW or LB broth) and working gas (air or helium). This can be explained by the fact that the increased applied voltage gives rise to higher electric fields, charged particle amounts, and RONS concentrations (and pH and conductivity), as shown in Figs. 6(a) and 7(a). All these factors contribute to the inactivation of *E. coli*.

Figure 12 shows the survival curves of *E. coli* under different helium contents in the air–helium mixture (applied voltage 18 kV, irradiation distance 3 mm). The treatment in ambient air with 2 slm helium addition exhibited a greater inactivation efficacy. Notably, helium contents higher than 2 slm into the DBD chamber did not lead to a higher inactivation efficacy. This result is in consistent with the changes in the RONS concentration [Fig. 6(b)], pH, and electrical conductivity [Fig. 7(b)] with varying helium addition. Interestingly, these are correlated with plasma properties such as excitation temperature (Fig. 5). The RONS, H<sub>2</sub>O<sub>2</sub>, NO<sub>2</sub><sup>−</sup>, and O<sub>3</sub>, concentrations (shown in Fig. 6) as well as the strong acidification detected in PT-DW (shown in Fig. 7) can partially explain this bactericidal activity.<sup>79</sup> Moreover, the results obtained for the air-only case revealed a difference in inactivation efficacy [shown in Fig. 10(c)], due to a different value of the initial bacterial concentration.

It should be noted that the levels of inactivation efficacy estimated in this study are slightly lower than those reported by Oehmigen *et al.*<sup>9</sup> This difference may be due to two reasons. The first concerns the power absorbed into plasma: Oehmigen *et al.* used a pulsed sinusoidal high voltage (20 kHz), where a 2.4 mJ energy was dissipated in each high-voltage cycle, whereas the power used in our experiment was much lower than that. The second reason is related to the volume of the solution. Our experiment used a two-times larger liquid volume than theirs, and the larger amounts of liquid present during the treatment suppressed bacterial inactivation. The amount of liquid present during plasma treatment *in vitro* is a key factor in mitigating short-lived species or other physical effects from plasmas. A DBD device such as the one presented in this study provides additional factors promoting bacterial inactivation, such as electroporation, UV radiation, charged particles, or short-lived species being decomposed in the absence of target cells.<sup>33</sup> For example, the DBD plasma may cause membrane lipid peroxidation,<sup>59</sup> enabling the penetration of reactive species into cells through a process similar to aquaporins,<sup>60</sup> a route potentially hindered by excess liquid. Moreover, short-wavelength UV radiation is efficiently scavenged by liquid layers;<sup>58</sup> accordingly, a larger liquid volume may lead to a reduced inactivation efficacy.

Figure 13 shows the *E. coli* reductions obtained under indirect PTL treatments. The operating parameters are; liquid volume 10 ml, air-helium 4 slm, applied voltage 18 kV, irradiation distance 3 mm. The inactivation efficiency of the PTL treatment was mainly influenced by the plasma treatment time. For the indirect treatment, a CFU reduction slightly higher than 2-log units was achieved upon 8 min of PT-DW treatment, denoting a much lower inactivation efficacy compared to the direct treatment. These results can be explained as follows: in the direct treatment, DBD plasma streamers come in direct contact with cells. This enhances the contribution of (low-range) UV radiation, electrical fields, and short-lived species to biological effects,<sup>33</sup> which may result in a more drastic microbial inactivation than indirect treatment. Furthermore, the inactivation efficiency of plasma-treated saline solution was observed to be slightly lower than that of PT-DW.<sup>9</sup>

Regardless of the treatment method, the most common forms of the microbial survival curves are exponential decay functions with single or multiple time constants.<sup>21</sup> The various compositions of the operating gas and power resulted in different log reduction values and CAP treatment times needed to achieve a desired level of inactivation. The combined action of RONS and pH was observed to play an important role in bacterial inactivation. The charged particles and the electric field might also play a significant role in direct CAP treatment. The inactivation mechanism of microorganisms by CAP is quite complex, and it is considered to involve the synergetic effect of reactive species, charged particles, and UV radiation.<sup>61</sup> The log reduction values of plasma inactivation can range from a couple of seconds to several minutes depending on the nature of the microorganisms, the type of medium supporting them, the initial concentration of the microorganism suspension, the microbial sample preparation method, the plasma exposure technique (remote or direct), and the treatment parameters.<sup>21,61</sup>

Many important aspects should be considered for scaling up the present technology, such as maximizing the production of available reactive species, achieving a large contact area between plasma and microorganisms, and realizing the optimum treatment conditions with respect to energy and inactivation efficiency.<sup>80</sup> A significant enhancement (of more than two orders of magnitude) in energy efficiency was observed for the nanosecond-pulsed DBD system presented in this study, compared to those utilizing sinusoidal and/or microsecond-pulsed high voltages.

## V. CONCLUSIONS

This study introduces a stable, diffuse, and unipolar nanosecond-pulsed DBD plasma with low gas temperature, which was produced by employing a multiple pin-to-plate electrode configuration. The physicochemical properties (pH and electrical conductivity) and concentrations of reactive species generated in the treated liquids (such as  $\text{H}_2\text{O}_2$ ,  $\text{NO}_2^-$ , and  $\text{O}_3$ , which play central roles in the aqueous-phase chemistry of plasma-treated liquids for bacterial inactivation) were measured as a function of the operating parameters. The nanosecond-pulsed DBD produced much higher RONS concentrations in a larger volume of liquid compared to those generated by low-frequency or microsecond-pulsed plasmas. Nanosecond-pulsed DBD enabled microbial inactivation over a larger area. The present investigation focused on the inactivation of multidrug-resistant *E. coli* bacteria in different media using a multiple pin-to-plate electrode-based DBD driven by a nanosecond-pulsed high voltage. We also investigated indirect treatment systems

by the plasma-treated liquids and their effect on *E. coli*-contaminated liquid samples. The log reduction value of the plasma inactivation method could range from a couple of seconds to several minutes depending on the plasma exposure method (indirect or direct) and the treatment parameters, as well as the type of medium supporting the microorganisms. The DBD treatment enabled microbial inactivation over a larger area. Different operating gas compositions and power levels led to different inactivation efficacies and log reduction values. The combined action of RONS and pH played an important role in bacterial inactivation. The gas composition inside the DBD chamber also affected the plasma characteristics and the properties of the treated liquids (and thus the antimicrobial efficacy of the PTL). A DBD plasma under a gas mixture of ambient air and 2 slm helium achieved an enhanced inactivation efficacy, which was correlated with the RONS concentration and pH in the plasma-treated liquids. In conclusion, large-area nanosecond-pulsed DBDs can be among ideal plasma systems for bacterial inactivation and liquid treatment on an industrial scale.

## ACKNOWLEDGMENTS

This work was supported by the National Research Foundation of Korea under Contract No. 2022R1A2C1006170. The authors are grateful to helpful suggestions by Professor S. M. Starikovskaia of Ecole Polytechnique in France, and Dr. D. C. Seo of Korea Fusion Energy Institute.

## AUTHOR DECLARATIONS

### Conflict of Interest

The authors have no conflicts to disclose.

### Author Contributions

**Min-Jeong Seong:** Investigation (equal). **Kyu-Ri Park:** Investigation (equal). **S. J. Kim:** Investigation (equal). **Hea-Min Joh:** Project administration (equal). **Hanul Moon:** Resources (equal). **T. Hun Chung:** Conceptualization (equal); Project administration (equal); Writing – original draft (equal).

## DATA AVAILABILITY

The data that support the findings of this study are available from the corresponding author upon reasonable request.

## REFERENCES

- <sup>1</sup>H.-E. Wagner, R. Brandenburg, K. V. Kozlov, A. Sonnenfeld, P. Michel, and J. F. Behnke, "The barrier discharge: Basic properties and applications to surface treatment," *Vacuum* **71**, 417 (2003).
- <sup>2</sup>J. H. Bae, J. J. Mun, M. J. Seong, S. J. Kim, H. M. Joh, and T. H. Chung, "Effects of duty ratio on liquid- and polymer-surface treatment by a unipolar microsecond-pulsed helium atmospheric-pressure plasma jet," *Phys. Plasmas* **30**, 043515 (2023).
- <sup>3</sup>D. Merche, N. Vandencastele, and F. Reniers, "Atmospheric plasmas for thin film deposition: A critical review," *Thin Solid Films* **520**, 4219 (2012).
- <sup>4</sup>P. S. Ganesh Subramanian, J. Ananthanarasimhan, P. Leelesh, H. Rao, A. M. Shivapuji, P.-L. Girard-Lauriault, and L. Rao, "Plasma-activated water from DBD as a source of nitrogen for agriculture: Specific energy and stability studies," *J. Appl. Phys.* **129**, 093303 (2021).

- <sup>5</sup>B. Adhikari, K. Pangomm, M. Veerana, S. Mitra, and G. Park, "Plant disease control by non-thermal atmospheric-pressure plasma," *Front. Plant Sci.* **11**, 77 (2020).
- <sup>6</sup>M. Ito, J.-S. Oh, T. Ohta, M. Shiratani, and M. Hori, "Current status and future prospects of agricultural applications using atmospheric-pressure plasma technologies," *Plasma Process. Polym.* **15**, e1700073 (2018).
- <sup>7</sup>Y.-M. Zhao, A. Patange, D.-W. Sun, and B. Tiwari, "Plasma-activated water: Physicochemical properties, microbial inactivation mechanisms, factors influencing antimicrobial effectiveness, and applications in the food industry," *Compr. Rev. Food Sci. Food Saf.* **19**, 3951–3979 (2020).
- <sup>8</sup>K. Oehmigen, M. Hähnel, R. Brandenburg, C. Wilke, K.-D. Weltmann, and T. von Woedtke, "The role of acidification for antimicrobial activity of atmospheric pressure plasma in liquids," *Plasma Process. Polym.* **7**, 250 (2010).
- <sup>9</sup>K. Oehmigen, J. Winter, M. Hähnel, C. Wilke, R. Brandenburg, K.-D. Weltmann, and T. von Woedtke, "Estimation of possible mechanisms of *Escherichia coli* inactivation by plasma treated sodium chloride solution," *Plasma Process. Polym.* **8**, 904 (2011).
- <sup>10</sup>J. Y. Park, S. Park, W. Choe, H. I. Yong, C. Jo, and K. Kim, "Plasma-functionalized solution: A potent antimicrobial agent for biomedical applications from antibacterial therapeutics to biomaterial surface engineering," *ACS Appl. Mater. Interfaces* **9**, 43470 (2017).
- <sup>11</sup>Y. Tan, Y. Bian, R. Fu, H. Niu, G. Chen, S. Li, and Y. Chen, "Potential use of plasma-activated water on *Escherichia coli* for sterilization: Efficacy and mechanism," *Plasma Process. Polym.* **21**, e2300095 (2024).
- <sup>12</sup>M. J. Traylor, M. J. Pavlovich, S. Karim, P. Hait, Y. Sakiyama, D. S. Clark, and D. B. Graves, "Long-term antibacterial efficacy of air plasma-activated water," *J. Phys. D: Appl. Phys.* **44**, 472001 (2011).
- <sup>13</sup>D. Xiao, C. Cheng, Y. Lan, G. H. Ni, J. Shen, Y. D. Meng, and P. K. Chu, "Effects of atmospheric-pressure nonthermal nitrogen and air plasma on bacteria inactivation," *IEEE Trans. Plasma Sci.* **44**, 2699 (2016).
- <sup>14</sup>H. Wang, L. Zhang, H. Luo, X. Wang, J. Tie, and Z. Ren, "Sterilizing processes and mechanisms for treatment of *Escherichia coli* with dielectric-barrier discharge plasma," *Appl. Environ. Microbiol.* **86**, e01907–19 (2019).
- <sup>15</sup>C. Jiang, E. B. Sözer, S. Song, N. Lai, P. T. Vernier, and S. Guo, "Modulation of ROS in nanosecond-pulsed plasma-activated media for dosage-dependent cancer cell inactivation in vitro," *Phys. Plasmas* **27**, 113513 (2020).
- <sup>16</sup>A. Lin, N. Chernets, J. Han, Y. Alicea, D. Dobrynin, G. Fridman, T. A. Freeman, A. Fridman, and V. Miller, "Non-equilibrium dielectric barrier discharge treatment of mesenchymal stem cells: Charges and reactive oxygen species play the major role in cell death," *Plasma Process. Polym.* **12**, 1117 (2015).
- <sup>17</sup>A. Lin, B. Truong, S. Patel, N. Kaushik, E. H. Choi, G. Fridman, A. Fridman, and V. Miller, "Nanosecond-pulsed DBD plasma-generated reactive oxygen species trigger immunogenic cell death in A549 lung carcinoma cells through intracellular oxidative stress," *Int. J. Mol. Sci.* **18**, 966 (2017).
- <sup>18</sup>L. Scally, S. Behan, A. M. Aguiar de Carvalho, C. Sarangapani, B. Tiwari, R. Malone, H. J. Byrne, J. Curtin, and P. J. Cullen, "Diagnostics of a large volume pin-to-plate atmospheric plasma source for the study of plasma species interactions with cancer cell cultures," *Plasma Process. Polym.* **18**, e2000250 (2021).
- <sup>19</sup>J. Kaupe, C. Y. T. Tschang, F. Birk, D. Coenen, M. H. Thoma, and S. Mitic, "Effect of cold atmospheric plasmas on bacteria in liquid: The role of gas composition," *Plasma Process. Polym.* **16**, 1800196 (2019).
- <sup>20</sup>U. Kogelschatz, "Dielectric-barrier discharges: Their history, discharge physics, and industrial applications," *Plasma Chem. Plasma Process.* **23**, 1 (2003).
- <sup>21</sup>K. G. Kostov, V. Rocha, C. Y. Koga-Ito, B. M. Matos, M. A. Algatti, R. Y. Honda, M. E. Kayama, and R. P. Mota, "Bacterial sterilization by a dielectric barrier discharge (DBD) in air," *Surf. Coat. Technol.* **204**, 2954 (2010).
- <sup>22</sup>F. Liu, G. Huang, and B. Ganguly, "Plasma excitation dependence on voltage slew rates in 10–200 Torr argon–nitrogen gas mixture DBD," *Plasma Sources Sci. Technol.* **19**, 045017 (2010).
- <sup>23</sup>Y. Sun, Y. Qiu, A. Nie, and X. Wang, "Experimental research on inactivation of bacteria by using dielectric barrier discharge," *IEEE Trans. Plasma Sci.* **35**, 1496 (2007).
- <sup>24</sup>S. Tao, L. Kaihua, Z. Cheng, Y. Ping, Z. Shichang, and P. Ruzheng, "Experimental study on repetitive unipolar nanosecond-pulse dielectric barrier discharge in air at atmospheric pressure," *J. Phys. D: Appl. Phys.* **41**, 215203 (2008).
- <sup>25</sup>D.-Z. Yang, W.-C. Wang, S. Z. Li, Y. Song, and D. X. Nie, "A diffusive air plasma in bi-directional nanosecond pulsed dielectric barrier discharge," *J. Phys. D: Appl. Phys.* **43**, 455202 (2010).
- <sup>26</sup>E. H. Arserim, D. Salvi, G. Fridman, D. W. Schafner, and M. V. Karwe, "Microbial inactivation by non-equilibrium short-pulsed atmospheric pressure dielectric barrier discharge (cold plasma): Numerical and experimental studies," *Food Eng. Rev.* **13**, 136 (2021).
- <sup>27</sup>S. Zhang, W. Wang, P. Jiang, D. Yang, L. Jia, and S. Wang, "Comparison of atmospheric air plasmas excited by high-voltage nanosecond pulsed discharge and sinusoidal alternating current discharge," *J. Appl. Phys.* **114**, 163301 (2013).
- <sup>28</sup>X. Zhang, B. J. Lee, H. G. Im, and M. S. Cha, "Ozone production with dielectric barrier discharge: Effects of power source and humidity," *IEEE Trans. Plasma Sci.* **44**, 2288 (2016).
- <sup>29</sup>L. Scally, J. Lalor, M. Gulan, P. J. Cullen, and V. Milosavljevic, "Spectroscopic study of excited molecular nitrogen generation due to interactions of metastable noble gas atoms," *Plasma Process. Polym.* **15**, 1800018 (2018).
- <sup>30</sup>S. Park, J. Kim, H. Lee, D. Han, S. Park, S. B. Kim, and W. Choe, "Nonheating ozone suppression in pulsed air discharges: Role of pulse duration and repetition rate," *J. Phys. D: Appl. Phys.* **54**, 394003 (2021).
- <sup>31</sup>J. M. Williamson, D. D. Trump, P. Bletzinger, and B. N. Ganguly, "Comparison of high-voltage ac and pulsed operation of a surface dielectric barrier discharge," *J. Phys. D: Appl. Phys.* **39**, 4400 (2006).
- <sup>32</sup>Y. Guo, M. Fang, L. Zhang, J. Sun, X. Wang, J. Tie, Q. Zhou, L. Zhang, and H. Luo, "Study on flexible surface dielectric barrier discharge plasma film for in situ inactivation of bacteria and viruses," *Appl. Phys. Lett.* **121**, 074101 (2022).
- <sup>33</sup>S. Bekechus, A. Lin, A. Fridman, K. Wende, K.-D. Weltmann, and V. Miller, "A comparison of floating-electrode DBD and kINPen Jet: Plasma parameters to achieve similar growth reduction in colon cancer cells under standardized conditions," *Plasma Chem. Plasma Process.* **38**(1), 1 (2018).
- <sup>34</sup>H. Ayan, G. Fridman, A. F. Gutsol, V. N. Vasilets, A. Fridman, and G. Friedman, "Nanosecond-pulsed uniform dielectric-barrier discharge," *IEEE Trans. Plasma Sci.* **36**, 504 (2008).
- <sup>35</sup>J. Ehlbeck, U. Schnabel, M. Polak, J. Winter, T. von Woedtke, R. Brandenburg, T. von dem Hagen, and K.-D. Weltmann, "Low temperature atmospheric pressure plasma sources for microbial decontamination," *J. Phys. D: Appl. Phys.* **44**, 013002 (2011).
- <sup>36</sup>K. Takaki, M. Hosokawa, T. Sasaki, S. Mukaigawa, and T. Fujiwara, "Production of atmospheric-pressure glow discharge in nitrogen using needle-array electrode," *Appl. Phys. Lett.* **86**, 151501 (2005).
- <sup>37</sup>D.-Z. Yang, W.-C. Wang, L. Jia, D.-X. Nie, and H.-C. Shi, "Production of atmospheric pressure diffuse nanosecond pulsed dielectric barrier discharge using the array needles-plate electrode in air," *J. Appl. Phys.* **109**, 073308 (2011).
- <sup>38</sup>L. Zhang, D.-Z. Yang, W.-C. Wang, Z.-J. Liu, S. Wang, P.-C. Jiang, and S. Zhang, "Atmospheric air diffuse array-needles dielectric barrier discharge excited by positive, negative, and bipolar nanosecond pulses in large electrode gap," *J. Appl. Phys.* **116**, 113301 (2014).
- <sup>39</sup>Z.-J. Liu, W.-C. Wang, D.-Z. Yang, S. Wang, S. Zhang, K. Tang, and P.-C. Jiang, "A large-area diffuse air discharge plasma excited by nanosecond pulse under a double hexagon needle-array electrode," *Spectrochim. Acta A: Mol. Biomol. Spectrosc.* **121**, 698 (2014).
- <sup>40</sup>Z.-J. Liu, W.-C. Wang, L. Zhang, S. Wang, D.-Z. Yang, S. Zhang, and K. Tang, "Electrical and optical characteristics of diffuse nanosecond pulsed discharge plasma using a needle-array electrode in atmospheric air," *J. Appl. Phys.* **115**, 203302 (2014).
- <sup>41</sup>S. P. Kalakonda, G. Parameswarreddy, E. N. Skariah, B. George, T. V. Suchithra, and T. K. Sindhu, "Treatment of *Escherichia coli* contaminated water with different pulse-powered NTP configurations and analysis for post treatment efficacy," *Sci. Rep.* **12**, 20380 (2022).
- <sup>42</sup>P. Lukes, E. Dolezalova, I. Sisrova, and M. Clupek, "Aqueous-phase chemistry and bactericidal effects from an air discharge plasma in contact with water: Evidence for the formation of peroxyxynitrite through a pseudo-second-order post-discharge reaction of H<sub>2</sub>O<sub>2</sub> and HNO<sub>2</sub>," *Plasma Sources Sci. Technol.* **23**, 015019 (2014).
- <sup>43</sup>J. H. Park, N. Kumar, D. H. Park, M. Yusupov, E. C. Neyts, C. C. W. Verlaack, A. Bogaerts, M. H. Kang, H. S. Uhm, E. H. Choi, and P. Attri, "A comparative

- study for the inactivation of multidrug resistance bacteria using dielectric barrier discharge and nano-second pulsed plasma." *Sci. Rep.* **5**, 13849 (2015).
- <sup>44</sup>V. S. Santosh, K. Kondeti, C. Q. Phan, K. Wende, H. Jablonowski, U. Gangal, J. L. Granick, R. C. Hunter, and P. J. Bruggeman, "Long-lived and short-lived reactive species produced by a cold atmospheric pressure plasma jet for the inactivation of *Pseudomonas aeruginosa* and *Staphylococcus aureus*," *Free Radical Biol. Med.* **124**, 275 (2018).
- <sup>45</sup>L. Guo, R. Xu, L. Gou, Z. Liu, Y. Zhao, D. Liu, L. Zhang, H. Chen, and M. G. Kong, "Mechanism of virus inactivation by cold atmospheric-pressure plasma and plasma-activated water," *Appl. Environ. Microbiol.* **84**, e00726–18 (2018).
- <sup>46</sup>A. L. V. Cubas, M. de Medeiros Machado, J. R. dos Santos, J. J. Zanco, D. H. B. Ribeiro, A. S. André, N. A. Debacher, and E. H. S. Moecke, "Effect of chemical species generated by different geometries of air and argon non-thermal plasma reactors on bacteria inactivation in water," *Sep. Purif. Technol.* **222**, 68 (2019).
- <sup>47</sup>M. Laroussi, X. Lu, and M. Keidar, "Perspective: The physics, diagnostics, and applications of atmospheric pressure low temperature plasma sources used in plasma medicine," *J. Appl. Phys.* **122**, 020901 (2017).
- <sup>48</sup>J. McKayla Nicol, T. R. Brubaker, B. J. Honish, II, A. N. Simmons, A. Kazemi, M. A. Geissel, C. T. Whalen, C. A. Siedlecki, S. G. Bilén, S. D. Knecht, and G. S. Kirimanjswara, "Antibacterial effects of low temperature plasma generated by atmospheric-pressure plasma jet are mediated by reactive oxygen species," *Sci. Rep.* **10**, 3066 (2020).
- <sup>49</sup>X. Lu and M. Laroussi, "Temporal and spatial emission behaviour of homogeneous dielectric barrier discharge driven by unipolar sub-microsecond square pulses," *J. Phys. D: Appl. Phys.* **39**, 1127 (2006).
- <sup>50</sup>M. Bogaczyk, G. B. Sretenović, and H.-E. Wagner, "Influence of the applied voltage shape on the barrier discharge operation modes in helium," *Eur. Phys. J. D* **67**, 212 (2013).
- <sup>51</sup>Z. Zhang, Z. Xu, C. Cheng, J. Wei, Y. Lan, G. Ni, Q. Sun, S. Qian, H. Zhang, W. Xia, J. Shen, Y. Meng, and P. K. Chu, "Bactericidal effects of plasma induced reactive species in dielectric barrier gas-liquid discharge," *Plasma Chem. Plasma Process.* **37**, 415 (2017).
- <sup>52</sup>R. Tschiersch, M. Bogaczyk, and H.-E. Wagner, "Systematic investigation of the barrier discharge operation in helium, nitrogen, and mixtures: Discharge development, formation and decay of surface charges," *J. Phys. D: Appl. Phys.* **47**, 365204 (2014).
- <sup>53</sup>E. Stoffels, A. J. M. Roks, and L. E. Deelmm, "Delayed effects of cold atmospheric plasma on vascular cells," *Plasma Process. Polym.* **5**, 599 (2008).
- <sup>54</sup>S. Liu and M. Neiger, "Excitation of dielectric barrier discharges by unipolar submicrosecond square pulses," *J. Phys. D: Appl. Phys.* **34**, 1632 (2001).
- <sup>55</sup>D. Pai, D. A. Lacoste, and C. O. Laux, "Images of nanosecond repetitively pulsed plasmas in preheated air at atmospheric pressure," *IEEE Trans. Plasma Sci.* **36**, 974 (2008).
- <sup>56</sup>C. Liu, A. Fridman, and D. Dobrynin, "Uniformity analysis of nanosecond and sub-nanosecond pulsed DBD in atmospheric air," *Plasma Res. Express* **1**, 015007 (2018).
- <sup>57</sup>M. Schmidt, V. Hahn, B. Altmann, T. Gerling, I. C. Gerber, K.-D. Weltmann, and T. von Woedtke, "Plasma-activation of larger liquid volumes by an inductively-limited discharge for antimicrobial purposes," *Appl. Sci.* **9**, 2150 (2019).
- <sup>58</sup>H. Jablonowski and T. von Woedtke, "Research on plasma medicine-relevant plasma-liquid interaction: What happened in the past five years?" *Clin. Plasma Med.* **3**, 42 (2015).
- <sup>59</sup>S. Ikawa, K. Kitano, and S. Hamaguchi, "Effects of pH on bacterial inactivation in aqueous solutions due to low-temperature atmospheric pressure plasma application," *Plasma Process. Polym.* **7**, 33 (2010).
- <sup>60</sup>D. Yan, A. Talbot, N. Nourmohammadi, J. H. Sherman, X. Cheng, and M. Keidar, "Toward understanding the selective anticancer capacity of cold atmospheric plasma—A model based on aquaporins (Review)," *Biointerphases* **10**, 040801 (2015).
- <sup>61</sup>S. Das, V. P. Gajula, S. Mohapatra, G. Singh, and S. Kar, "Role of cold atmospheric plasma in microbial inactivation and the factors affecting its efficacy," *Health Sci. Rev.* **4**, 100037 (2022).
- <sup>62</sup>K. Stapelmann, S. Gershman, and V. Miller, "Plasma-liquid interactions in the presence of organic matter—A perspective," *J. Appl. Phys.* **135**, 160901 (2024).
- <sup>63</sup>I. Schweigert, A. Alexandrov, D. Zakrevsky, P. Gugin, E. Milakhina, E. Golubitskaya, O. Troitskaya, M. Biryukov, and O. Koval, "Analysis of grounded substrate effects on cold atmospheric plasma jet irradiation of cellular and animal models," *J. Phys.: Conf. Ser.* **1698**, 012010 (2020).
- <sup>64</sup>M. Klas and S. Ptasinska, "Characteristics of N<sub>2</sub> and N<sub>2</sub>/O<sub>2</sub> atmospheric pressure glow discharges," *Plasma Sources Sci. Technol.* **22**, 025013 (2013).
- <sup>65</sup>X. Duten, D. Packan, L. Yu, C. O. Laux, and C. H. Kruger, "DC and pulsed glow discharges in atmospheric pressure air and nitrogen," *IEEE Trans. Plasma Sci.* **30**, 178 (2002).
- <sup>66</sup>T. Kawasaki, S. Kusumegi, A. Kudo, T. Sakanoshita, T. Tsurumaru, A. Sato, G. Uchida, K. Koga, and M. Shiratani, "Effects of irradiation distance on supply of reactive oxygen species to the bottom of a Petri dish filled with liquid by an atmospheric O<sub>2</sub>/He plasma jet," *J. Appl. Phys.* **119**, 173301 (2016).
- <sup>67</sup>K. Grosse, J. Held, M. Kai, and A. von Keudell, "Nanosecond plasmas in water: Ignition, cavitation and plasma parameters," *Plasma Sources Sci. Technol.* **28**, 085003 (2019).
- <sup>68</sup>C. Ding, A. Khomenko, S. A. Shcherbanev, and S. M. Starikovskaia, "Filamentary nanosecond surface dielectric barrier discharge. Experimental comparison of the streamer-to-filament transition for positive and negative polarities," *Plasma Sources Sci. Technol.* **28**, 085005 (2019).
- <sup>69</sup>A. Khomenko, V. Podolsky, and X. X. Wang, "Different approaches of measuring high-voltage nanosecond pulses and power delivery in plasma systems," *Electr. Eng.* **103**, 57 (2021).
- <sup>70</sup>J. Y. Park, J. H. Bae, and S. Lee, "Characteristics of aqueous chemical species generation in plasma-facing liquid systems using helium jet plasma," *ChemistryOpen* **13**, e202300213 (2024).
- <sup>71</sup>R. K. Gangwar, O. Levasseur, N. Naudé, N. Gherardi, F. Massines, J. Margot, and L. Stafford, "Determination of the electron temperature in plane-to-plane He dielectric barrier discharges at atmospheric pressure," *Plasma Sources Sci. Technol.* **25**, 015011 (2016).
- <sup>72</sup>Z. Machala, B. Tarabova, K. Hensel, E. Spetlikova, L. Sikurova, and P. Lukes, "Formation of ROS and RNS in water electro-sprayed through transient spark discharge in air and their bactericidal effects," *Plasma Process. Polym.* **10**, 649 (2013).
- <sup>73</sup>I.-E. Vlad and S. D. Anghel, "Time stability of water activated by different on liquid atmospheric pressure plasmas," *J. Electroanal. Chem.* **87**, 284 (2017).
- <sup>74</sup>A. Jo, H. M. Joh, J. H. Bae, S. J. Kim, T. H. Chung, and J. W. Chung, "Plasma activated medium prepared by a bipolar microsecond-pulsed atmospheric pressure plasma jet array induces mitochondria-mediated apoptosis in human cervical cancer cells," *PLoS One* **17**, e0272805 (2022).
- <sup>75</sup>O. van Rooij, O. Ahlborn, and A. Sobota, "Electron density in a non-thermal atmospheric discharge in contact with water and the effect of water temperature on plasma-water interactions," *J. Phys. D: Appl. Phys.* **57**, 385206 (2024).
- <sup>76</sup>L. Chandana, C. J. Sangeetha, T. Shashidhar, and C. Subrahmanyam, "Non-thermal atmospheric pressure plasma jet for the bacterial inactivation in an aqueous medium," *Sci. Total Environ.* **640–641**, 493 (2018).
- <sup>77</sup>A. Lavrikova, N. C. T. Dadi, H. Bujdaková, and K. Hensel, "Inactivation pathways of *Escherichia coli* and *Staphylococcus aureus* induced by transient spark discharge in liquids," *Plasma Process. Polym.* **21**, e2300147 (2024).
- <sup>78</sup>T. von Woedtke, S. Reuter, K. Masur, and K.-D. Weltmann, "Plasmas for medicine," *Phys. Rep.* **530**, 291 (2013).
- <sup>79</sup>N. Iwata, V. Gamaleev, J. -S. Oh, T. Ohta, M. Hori, and M. Ito, "Investigation on the long-term bactericidal effect and chemical composition of radical-activated water," *Plasma Process. Polym.* **16**, e1900055 (2019).
- <sup>80</sup>I. A. Hamza, A. S. El-Kalliny, S. Abd-Elmaksoud, M. A. Marouf, M. S. Abdel-Wahed, M. A. El-Liethy, and M. M. Hefny, "Cold atmospheric plasma: A sustainable approach to inactivating viruses, bacteria, and protozoa with remediation of organic pollutants in river water and wastewater," *Environ. Sci. Pollut. Res.* **30**, 116214 (2023).